Supplement of Nat. Hazards Earth Syst. Sci., 26, 2031–2050, 2026
https://doi.org/10.5194/nhess-26-2031-2026-supplement

Natural Hazards and Earth System Sciences
Open Access
EGU

Supplement of

Non-stationary dynamics of compound climate extremes: a WRF-CMIP6-GAMLSS framework for southeastern China

Yinchi Zhang et al.

Correspondence to: Lu Gao (l.gao@foxmail.com)

Methods

S1. Empirical Mode Decomposition (EMD)

Empirical Mode Decomposition (EMD) is a data-driven technique used to decompose a signal into a set of intrinsic mode functions (IMFs) and a residual trend (Huang et al., 1998). It is particularly suitable for analyzing nonlinear and non-stationary time series data. Many studies have shown that the residuals of EMD can reflect the deterministic trend of non-stationary sequences (Lee and Ouarda, 2010; Qian, 2016; Wu et al., 2023). In this study, the EMD is applied to quantify the deterministic trends in the recurrence hazards of compound extreme events. The formula is as follows:

$$x(t) = \sum_{i=1}^{n} IMF_i(t) + r_n(t)$$

$x(t)$ is the original signal. $IMF_i(t)$ represents the i-th intrinsic mode function, which is the result of the decomposition. $r_n(t)$ is the residual (a trend or constant component left after the decomposition). Typically, it is a constant or a slowly varying trend.

Results

S1 Assessing the regional applicability of downscaled CMIP6bc based on historical data

Although the quality of CMIP6bc has been widely validated across China, a regional applicability assessment remains necessary. Table S3 presents the specific information for each station, Table S4 and S5 show the simulated temperature results from CMIP6bc and ERA5, and Table S6 and S7 display the simulated precipitation results. The spatial patterns of precipitation and temperature (Figures S1 a–f) are constructed by performing spline interpolation on the observed data from the 30 stations in the MRB using Arc Geographic Information System (ArcGIS). It represents the interpolated annual mean values at each meteorological station and the nearest WRF grid point over the 10-year historical period. To eliminate the interpolation errors, we extracted the nearest WRF grid points for each meteorological station and compared them by plotting a Taylor diagram (Figures S1 i-l). We evaluate the simulation performance of precipitation and temperature using Correlation Coefficient (CC), Percent Bias (PBIAS), Root Mean Square Error (RMSE), and Standard Deviation (STD) (Table S8). CC and PBIAS represent the averages across all stations, whereas in the Taylor diagrams, CC, RMSE, and STD are calculated based on the nearest WRF grid point to each station. Compared to observations, both the downscaled ERA5 and CMIP6bc demonstrated satisfactory performance in reproducing the spatio-temporal distribution

characteristics of precipitation and temperature across the MRB. Specifically, the ERA5-based simulations outperform CMIP6bc, particularly for precipitation (CC = 0.88, PBIAS = 3.79%) compared to temperature (CC = 0.80; PBIAS = 4.03%). However, the models demonstrate consistent underestimations in the downstream areas and overestimations in the northwestern Wuyi Mountain region. These systematic biases are likely attributable to orographic effects, with the WRF model consistently underestimating precipitation in plain areas while overestimating it in high-elevation regions (Wang et al., 2020; Min et al., 2021). As shown in Figures S1 (g, h), the results from both driving datasets capture the observed temporal variations, with temperature simulations showing better agreement than precipitation. The Taylor diagrams reveal that the WRF model's performance is comparatively weaker in the downstream sub-basin of the MRB than the other three sub-basins. High-altitude areas typically experience stronger radiation effects, especially in mountainous regions with thinner atmospheres. The WRF model may have errors in simulating radiation transfer, leading to temperatures in high-altitude areas being lower than actual conditions (Varga et al., 2020). In addition, the downstream area of the MRB is an urban agglomeration, where urban areas typically experience stronger radiation and heat accumulation effects. These effects may not be fully accounted for in the model, leading to simulated temperatures being higher than actual conditions (Chen et al., 2025). In summary, although CMIP6bc underperforms ERA5 due to resolution limitations, it still exhibits reasonable spatio-temporal consistency with the observations. We conclude that such discrepancies remain within an acceptable range for subsequent research.

S2 WRF parametrization scheme sensitivity experiments.

In our previous study, we conducted a detailed sensitivity analysis and optimization of parameterization schemes specifically for the MRB (Lin et al., 2023). We focused on two schemes that have the most significant impact on precipitation: microphysics and cumulus convection. By cross-combining these schemes, we developed 16 combinations (as shown in Table S9) and assessed their performance in simulating precipitation across different magnitudes. Through a comprehensive evaluation of the temporal (Figure S2 and Figure S3) and spatial (Figure S4 and Table S10) characteristics, we determined that the 9th configuration (Lin and NT) is the most suitable for simulating extreme precipitation events in the MRB. As a result, this configuration was adopted in the present study to ensure the most accurate simulation of extreme precipitation events in this region.

Table

Table S1 CMIP6 models used in CMIP6bc.

No.	Model	Institution	Approximate grid spacing
1	ACCESS-CM2	Commonwealth Scientific and Industrial Research Organisation (Australia)	1.875° × 1.25°
2	ACCESS-ESM1–5	Commonwealth Scientific and Industrial Research Organisation (Australia)	1.875° × 1.25°
3	CanESM5	Canadian Centre for Climate Modelling and Analysis (Canada)	2.81° × 2.81°
4	BCC-CSM2-MR	Beijing Climate Center (China)	1.125° × 1.125°
5	FGOALS-f3-L	Institute of Atmospheric Physics, Chinese Academy of Sciences (China)	1.25° × 1°
6	FGOALS-g3	Institute of Atmospheric Physics, Chinese Academy of Sciences (China)	2° × 2.25°
7	EC-Earth3	European EC-Earth Consortium (Europe)	0.70° × 0.70°
8	EC-Earth3-Veg	European EC-Earth Consortium (Europe)	0.70° × 0.70°
9	IPSL-CM6A-LR	Institute Pierre Simon Laplace (France)	2.5° × 1.26°
10	AWI-CM-1-1-MR	Alfred Wegener Institute, Helmholtz Centre for Polar and Marine Research (Germany)	0.94° × 0.94°
11	MPI-ESM1-2-HR	Max Planck Institute for Meteorology (Germany)	0.94° × 0.94°
12	MPI-ESM1-2-LR	Max Planck Institute for Meteorology (Germany)	1.875° × 1.875°
13	MIROC6	Japan Agency for Marine-Earth Science and Technology (Japan)	1.41° × 1.41°
14	MRI-ESM2-0	Meteorological Research Institute, Japan Meteorological Agency (Japan)	1.125° × 1.125°
15	NorESM2-LM	Norwegian Climate Center (Norway)	2.5° × 1.875°
16	CESM2	Climate and Global Dynamics Laboratory, National Center for Atmospheric Research (USA)	1.25° × 0.94°
17	CESM2-WACCM	Climate and Global Dynamics Laboratory, National Center for Atmospheric Research (USA)	1.25° × 0.94°
18	GFDL-ESM4	Geophysical Fluid Dynamics Laboratory, National Oceanic and Atmosphere Administration (USA)	1.25° × 1.0°

63 Table S2 Distribution functions in this study.

Distribution function	Abbreviation	Number of parameters
Gamma	GA	2
Gumbel	GU	2
Inverse Gamma	IGAMMA	2
Inverse Gaussian	IG	2
Logistic	LO	2
Log-Normal	LOGNO	2
Reverse Gumbel	RG	2
Weibull	WEI3	2
Normal	NO	2
Exponential gen. beta 2	EGB2	4
Johnson's SU repar.	JSU	4
Johnson's original SU	JSUo	4
Generalised t	GT	4
SU	SU	4
NET	NET	4
Sinh-arcsinh	SHASH	4
Sinh-arcsinh original	SHASHo	4
Sinh-arcsinh original 2	SHASHo2	4

64

Table S3 Meteorological stations information.

ID	Name	Longitude (°N)	Latitude (°E)	Elevation (m)
1	Jiuxianshan	118.1	25.72	1653.5
2	Gutian	118.73	26.58	361.5
3	Datian	117.83	25.7	400.1
4	Youxi	118.15	26.17	126.1
5	Dehua	118.23	25.48	521.4
6	Yongtai	118.93	25.87	85.6
7	Fuzhou	119.28	26.08	83.8
8	Changle	119.5	25.97	4.1
9	Minhou	119.15	26.15	57.8
10	Minqing	118.85	26.23	40.8
11	Sanming	117.62	26.27	215
12	Ninghua	116.63	26.23	358.9
13	Yongan	117.35	25.97	206
14	Shaxian	117.8	26.4	120.6
15	Qingliu	116.85	26.2	310.6
16	Liancheng	116.75	25.72	380.0
17	Guangze	117.3	27.52	265.4
18	Nanping	118.17	26.65	125.6
19	Jiangle	117.47	26.73	154.7
20	Jianning	116.85	26.83	342.3
21	Shaxi	117.15	26.4	357.4
22	Taining	117.17	26.9	342.9
23	Shaowu	117.47	27.33	191.5
24	Shunchang	117.8	26.8	175.2
25	Jianou	118.31	27.05	154.9
26	Jianyang	118.12	27.33	196.9
27	Zhenghe	118.82	27.37	221.5
28	Songxi	118.8	27.52	205.4
29	Wuyishan	118.03	27.77	220.6
30	Pucheng	118.53	27.92	276.9

Table S4 Temperature simulation results based on ERA5

Station	STD	RMSE	CC
Jiuxianshan	1.14	0.59	0.99
Gutian	0.98	0.29	0.99
Datian	0.97	0.07	1.00
Youxi	0.99	0.23	0.99
Dehua	0.98	0.20	0.99
Yongtai	1.00	0.22	0.99
Fuzhou	0.97	0.26	0.98
Changle	0.92	0.20	0.98
Minhou	0.97	0.35	0.95
Minqing	0.98	0.16	0.99
Sanming	1.03	0.30	0.99
Ninghua	0.99	0.12	0.99
Yongan	1.01	0.32	0.99
Shaxian	1.03	0.36	0.99
Qingliu	0.96	0.14	0.99
Liancheng	1.01	0.27	0.99
Guangze	1.01	0.19	0.99
Nanping	1.02	0.29	0.99
Jiangle	1.02	0.29	0.99
Jianning	1.02	0.19	0.99
Shaxi	0.97	0.26	0.99
Taining	0.99	0.21	0.99
Shaowu	1.03	0.31	0.99
Shunchang	1.03	0.32	0.99
Jianou	0.78	0.25	0.99
Jianyang	0.75	0.36	0.99
Zhenghe	1.01	0.14	0.99
Songxi	0.99	0.14	0.99
Wuyishan	0.82	0.27	1.00
Pucheng	1.05	0.26	0.99

Table S5 Temperature simulation results based on CMIP6bc

Station	STD	RMSE	CC
Jiuxianshan	1.10	0.66	0.96
Gutian	0.96	0.37	0.97
Datian	0.94	0.29	0.96
Youxi	0.95	0.30	0.96
Dehua	0.97	0.30	0.96
Yongtai	0.96	0.29	0.96
Fuzhou	0.96	0.32	0.96
Changle	0.88	0.28	0.96
Minhou	0.53	0.68	0.96
Minqing	0.94	0.27	0.96
Sanming	0.97	0.37	0.96
Ninghua	0.93	0.25	0.97
Yongan	0.95	0.30	0.96
Shaxian	0.96	0.33	0.97
Qingliu	0.91	0.26	0.97
Liancheng	0.93	0.32	0.96
Guangze	0.96	0.28	0.98
Nanping	0.98	0.37	0.97
Jiangle	0.95	0.27	0.97
Jianning	0.96	0.28	0.98
Shaxi	0.92	0.33	0.97
Taining	0.94	0.28	0.97
Shaowu	0.95	0.27	0.97
Shunchang	0.95	0.30	0.97
Jianou	0.79	0.32	0.97
Jianyang	0.73	0.41	0.97
Zhenghe	0.95	0.25	0.97
Songxi	0.94	0.25	0.97
Wuyishan	0.81	0.35	0.97
Pucheng	0.95	0.24	0.98

Table S6 Precipitation simulation results based on ERA5

Station	STD	RMSE	CC
Jiuxianshan	1.20	0.71	0.80
Gutian	1.13	0.55	0.87
Datian	1.20	0.71	0.81
Youxi	1.35	0.72	0.86
Dehua	1.16	0.64	0.83
Yongtai	1.04	0.69	0.78
Fuzhou	0.94	0.75	0.74
Changle	0.76	0.89	0.62
Minhou	1.04	0.79	0.73
Minqing	1.10	0.65	0.81
Sanming	0.98	0.61	0.81
Ninghua	1.18	0.74	0.78
Yongan	1.12	0.61	0.84
Shaxian	0.97	0.56	0.84
Qingliu	1.16	0.72	0.79
Liancheng	1.36	0.89	0.75
Guangze	1.24	0.51	0.92
Nanping	0.97	0.53	0.85
Jiangle	1.07	0.45	0.91
Jianning	1.12	0.69	0.79
Shaxi	1.01	0.57	0.84
Taining	1.11	0.46	0.91
Shaowu	1.35	0.82	0.80
Shunchang	1.06	0.51	0.88
Jianou	0.96	0.54	0.85
Jianyang	0.99	0.46	0.89
Zhenghe	1.06	0.44	0.91
Songxi	1.17	0.55	0.89
Wuyishan	1.23	0.48	0.93
Pucheng	1.06	0.59	0.84

73 Table S7 Precipitation simulation results based on CMIP6bc

Station	STD	RMSE	CC
Jiuxianshan	1.19	0.98	0.61
Gutian	1.12	0.92	0.63
Datian	1.38	1.05	0.65
Youxi	1.11	0.85	0.68
Dehua	1.06	0.83	0.69
Yongtai	0.94	0.97	0.52
Fuzhou	0.94	0.94	0.57
Changle	0.82	0.70	0.73
Minhou	0.93	0.96	0.54
Minqing	1.16	0.97	0.60
Sanming	1.10	0.84	0.68
Ninghua	1.12	0.81	0.71
Yongan	1.26	1.04	0.59
Shaxian	0.97	0.82	0.66
Qingliu	1.23	0.98	0.63
Liancheng	1.31	1.11	0.56
Guangze	1.13	0.86	0.68
Nanping	0.98	0.75	0.71
Jiangle	1.13	0.84	0.69
Jianning	1.06	0.88	0.64
Shaxi	1.26	0.96	0.67
Taining	1.16	0.89	0.66
Shaowu	1.15	0.92	0.64
Shunchang	1.11	0.78	0.73
Jianou	1.01	0.80	0.68
Jianyang	1.13	0.89	0.65
Zhenghe	1.11	0.96	0.59
Songxi	1.15	0.90	0.66
Wuyishan	1.18	0.83	0.72
Pucheng	1.11	0.80	0.71

74

Table S8 Definition of evaluation criteria.

Metric	Formula	Optimal value	Range
CC	$CC = \frac{\sum_{i=1}^{n}(O_i - \overline{O_i})(M_i - \overline{M_i})}{\sqrt{\sum_{i=1}^{n}(O_i - \overline{O_i})^2}\sqrt{\sum_{i=1}^{n}(M_i - \overline{M_i})^2}}$	1	(0, 1)
PBIAS	$PBIAS = \sum_{i=1}^{n} \frac{M_i - O_i}{O_i}$	0	(-∞, +∞)
RMSE	$RMSE = \sqrt{\frac{1}{n}\sum_{i=1}^{n}(M_i - O_i)}$	0	(0, +∞)
STD	$STD = \sqrt{\frac{1}{n}\sum_{i=1}^{n}(O_i - \bar{O})^2}$	0	(0, +∞)

Notes: Where O_i presents meteorological data at the i station, M_i presents data at the WRF grid point closest to the i station, n is the numbers of stations.

Table S9 Parameterization scheme combinations design.

Combinations	Microphysics scheme (MP)	Cumulus scheme (CU)
EXP1	WSM6	Betts-Miller-Janjic (BMJ)
EXP2	WSM6	Betts-Miller-Janjic (BMJ)
EXP3	WSM6	Betts-Miller-Janjic (BMJ)
EXP4	WSM6	Betts-Miller-Janjic (BMJ)
EXP5	WDM6	Kain-Fritsch (KF)
EXP6	WDM6	Kain-Fritsch (KF)
EXP7	WDM6	Kain-Fritsch (KF)
EXP8	WDM6	Kain-Fritsch (KF)
EXP9	Purdue Lin (Lin)	New Tiedtke (NT)
EXP10	Purdue Lin (Lin)	New Tiedtke (NT)
EXP11	Purdue Lin (Lin)	New Tiedtke (NT)
EXP12	Purdue Lin (Lin)	New Tiedtke (NT)
EXP13	Thompson	Grell-Devenyi (GD)
EXP14	Thompson	Grell-Devenyi (GD)
EXP15	Thompson	Grell-Devenyi (GD)
EXP16	Thompson	Grell-Devenyi (GD)

Table S10 Evaluation metrics for total accumulated precipitation

Combination	TS (light)	TS (moderate)	TS (heavy)	TS (torrential)	$\overline{TS}$	$\overline{POD}$	$\overline{FAR}$
EXP1	0.22	0.11	0.07	0.15	0.14	0.24	0.71
EXP2	0.22	0.10	0.14	0.08	0.14	0.24	0.69
EXP3	0.24	0.11	0.09	0.16	0.15	0.27	0.66
EXP4	0.22	0.05	0.14	0.14	0.14	0.25	0.70
EXP5	0.14	0.07	0.07	0.11	0.10	0.16	0.71
EXP6	0.12	0.09	0.09	0.07	0.09	0.15	0.74
EXP7	0.18	0.09	0.10	0.12	0.12	0.20	0.64
EXP8	0.16	0.09	0.11	0.14	0.12	0.19	0.68
EXP9	0.26	0.11	0.12	0.16	0.16	0.29	0.66
EXP10	0.22	0.10	0.11	0.11	0.14	0.24	0.74
EXP11	0.24	0.12	0.13	0.14	0.16	0.23	0.55
EXP12	0.25	0.10	0.10	0.13	0.15	0.24	0.71
EXP13	0.22	0.10	0.07	0.11	0.12	0.21	0.67
EXP14	0.21	0.08	0.08	0.06	0.11	0.20	0.74
EXP15	0.24	0.09	0.10	0.13	0.14	0.25	0.70
EXP16	0.24	0.12	0.13	0.12	0.15	0.26	0.67

Note: TS (light rain, moderate rain, heavy rain, torrential rain) refers to the average of daily 24-hour accumulated precipitation. $\overline{TS}$, $\overline{POD}$ and $\overline{FAR}$ represent the average values of the scores for the four precipitation levels.

Figure

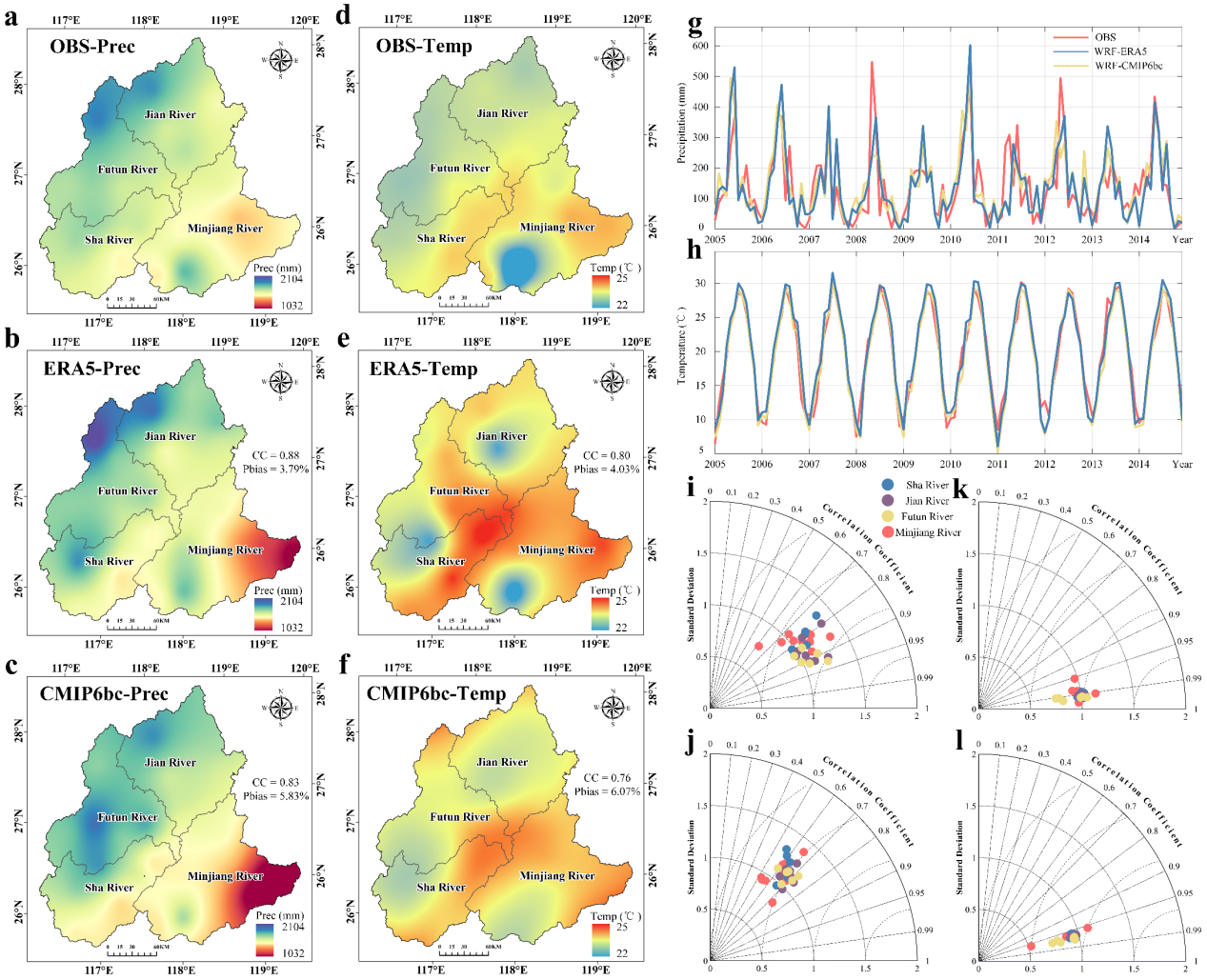

Figure S1. Evaluation of WRF-simulated precipitation and temperature over the MRB (2005-2014). spatial patterns of precipitation (a–c), temperature (d–f). Temporal evolution of precipitation (g) and temperature (h). Panels (i–l) present sub-basin comparisons of precipitation and temperature from ERA5 (i, k) and CMIP6bc (j, l).

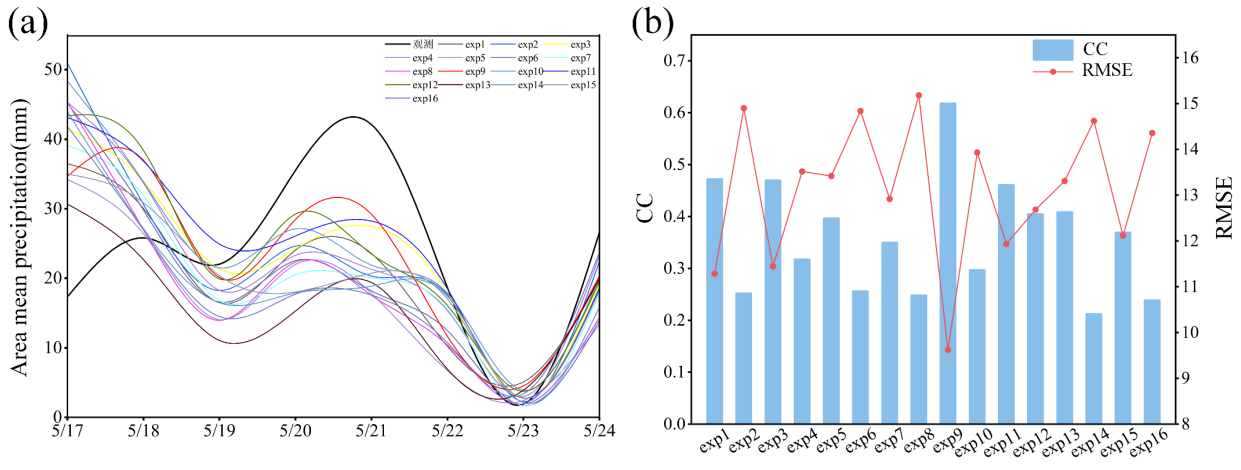

Figure S2. Time series of observations and WRF simulation.

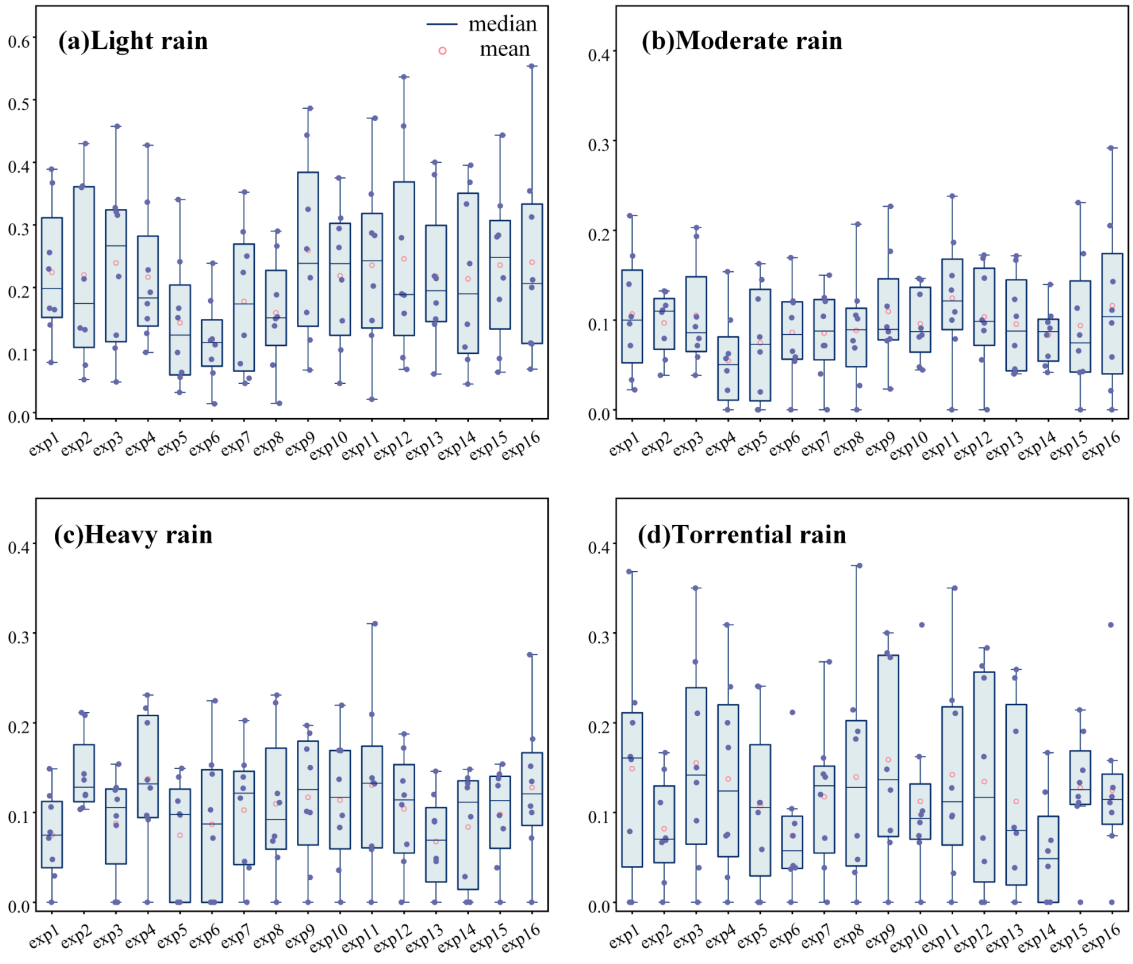

Figure S3. Box plot of TS scores for 24-hour accumulated precipitation simulated by WRF.

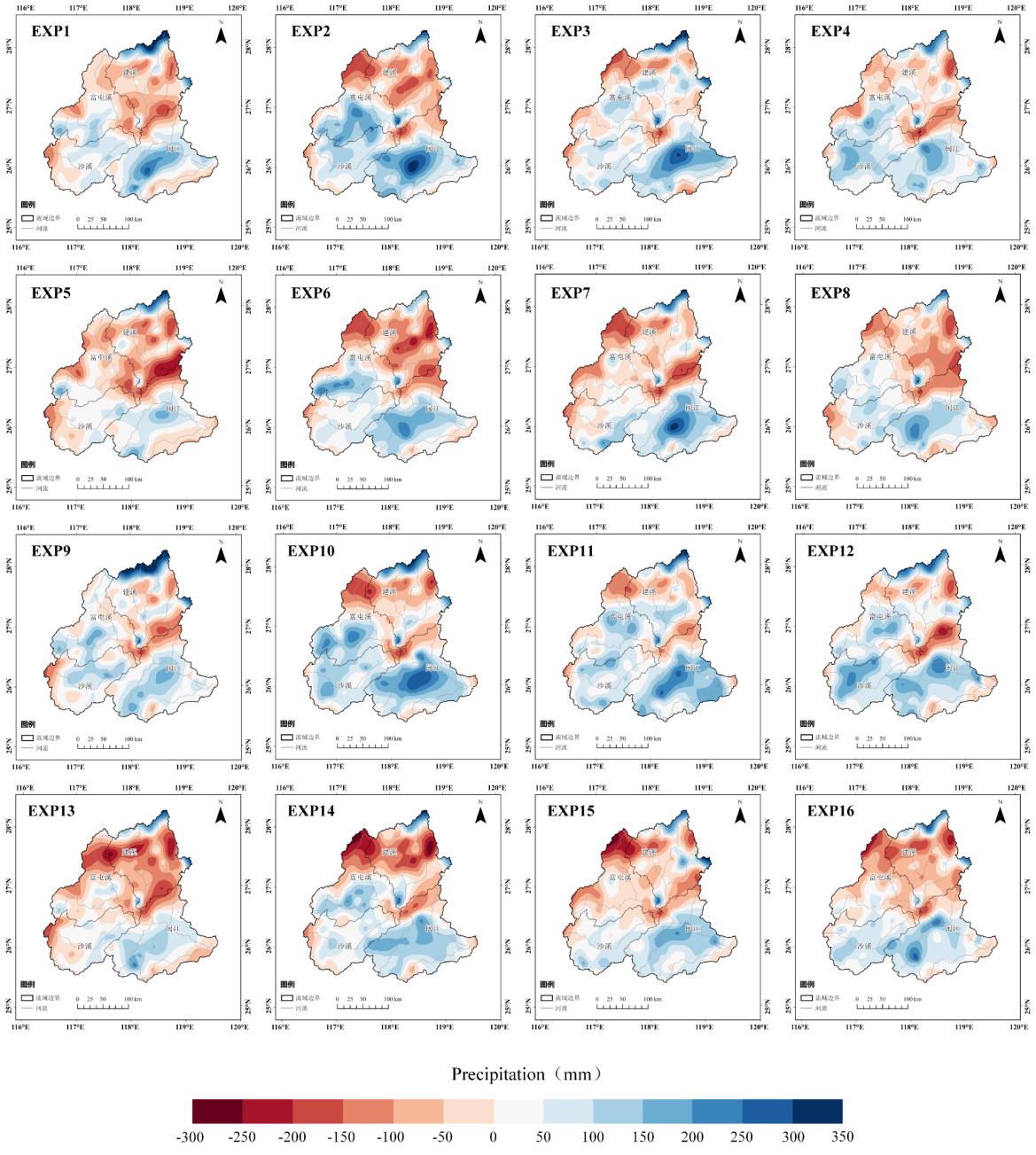

94

95 Figure S4. Spatial distribution of biases of total accumulated precipitation from WRF

96 parametrization scheme sensitivity experiments.

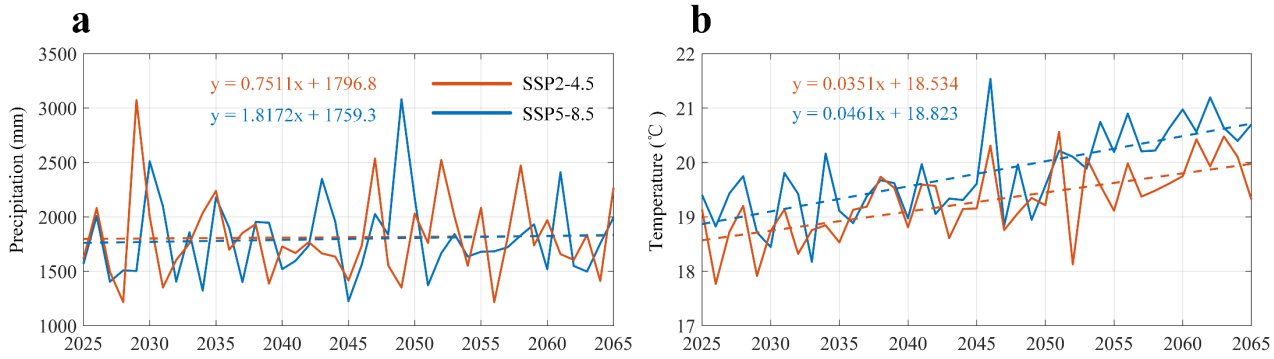

97

98 Figure S5. Variation of in annual precipitation (a) and temperature (b) in MRB from 2025 to 2065.

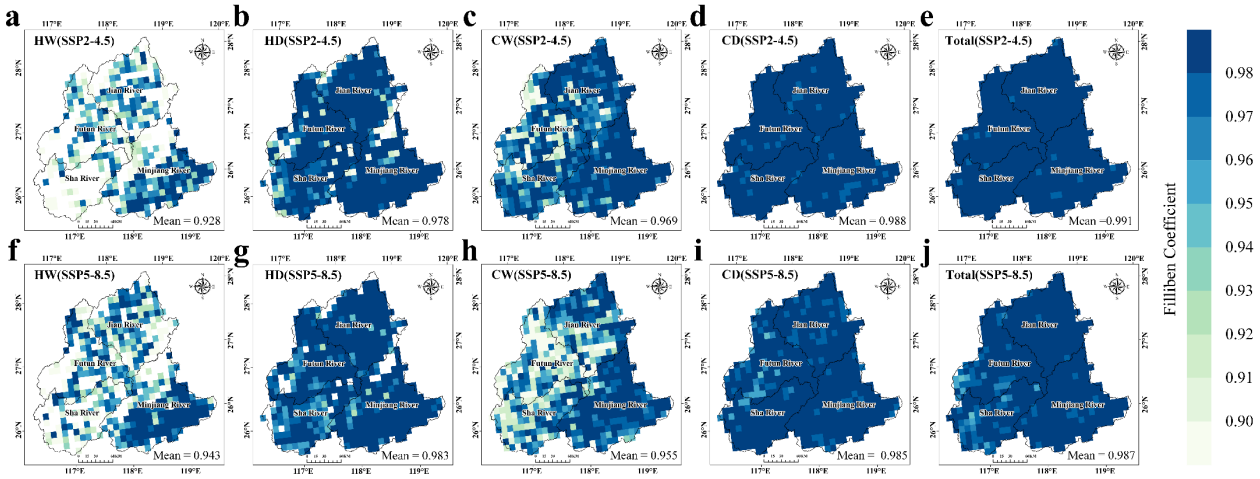

Figure S6. Maps of the Filliben Coefficient for CCEs.

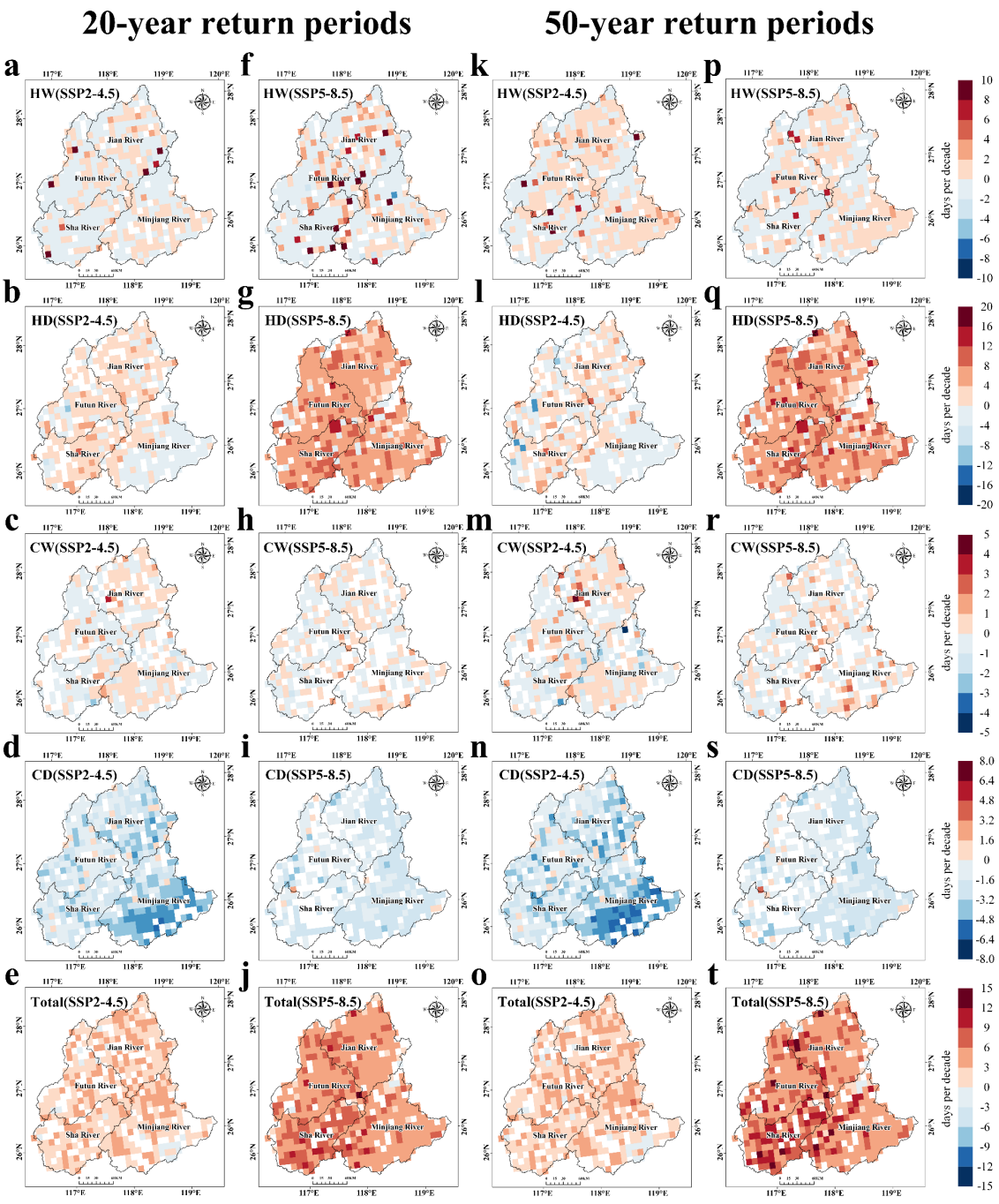

Figure S7. As in Figure 7 but for 20- and 50- return periods.

References

Chen, G., Mei, S.-J., Hang, J., Li, Q., and Wang, X.: URANS simulations of urban microclimates: Validated by scaled outdoor experiments, Building and Environment, 272, 112691, https://doi.org/10.1016/j.buildenv.2025.112691, 2025.

Huang, N. E., Shen, Z., Long, S. R., Wu, M. C., Shih, H. H., Zheng, Q., Yen, N.-C., Tung, C. C., and Liu, H. H.: The empirical mode decomposition and the Hilbert spectrum for nonlinear and non-stationary time series analysis, Proc. R. Soc. Lond. A, 454, 903–995, https://doi.org/10.1098/rspa.1998.0193, 1998.

Lee, T. and Ouarda, T. B. M. J.: Long - term prediction of precipitation and hydrologic extremes with nonstationary oscillation processes, J. Geophys. Res., 115, 2009JD012801, https://doi.org/10.1029/2009JD012801, 2010.

Lin, S., Zhang, Y., Sun, S., Guan, X., Jiang, C., Gao, L.: Sensitivity study of WRF parameterization schemes and initial fields on simulation of rainstorm in the Minjiang River basin. Pearl River (in Chinese) 44(10):35-46+61. https://doi: 10.3969/j.issn.1001-9235.2023.10.004, 2023.

Min, Y., Huang, W., Ma, M., and Zhang, Y.: Simulations in the Topography Effects of Tianshan Mountains on an Extreme Precipitation Event in the Ili River Valley, China, Atmosphere, 12, 750, https://doi.org/10.3390/atmos12060750, 2021.

Qian, C.: On trend estimation and significance testing for non-Gaussian and serially dependent data: quantifying the urbanization effect on trends in hot extremes in the megacity of Shanghai, Clim. Dyn., 47, 329–344, https://doi.org/10.1007/s00382-015-2838-0, 2016.

Varga, Á. J. and Breuer, H.: Sensitivity of simulated temperature, precipitation, and global radiation to different WRF configurations over the Carpathian Basin for regional climate applications, Clim. Dyn., 55, 2849–2866, https://doi.org/10.1007/s00382-020-05416-x, 2020.

Wang, Y., Yang, K., Zhou, X., Chen, D., Lu, H., Ouyang, L., Chen, Y., Lazhu, and Wang, B.: Synergy of orographic drag parameterization and high resolution greatly reduces biases of WRF-simulated precipitation in central Himalaya, Clim. Dyn., 54, 1729–1740, https://doi.org/10.1007/s00382-019-05080-w, 2020.

Wu, J., Wang, Z., Dong, J., Cui, X., Tao, S., and Chen, X.: Robust Runoff Prediction with Explainable Artificial Intelligence and Meteorological Variables from Deep Learning Ensemble Model, Water Resour. Res., 59, e2023WR035676, https://doi.org/10.1029/2023WR035676, 2023b.